iJRASET
International Journal For Research in Applied Science and Engineering Technology

INTERNATIONAL JOURNAL FOR RESEARCH

IN APPLIED SCIENCE & ENGINEERING TECHNOLOGY

Volume: 11 **Issue:** VIII **Month of publication:** Aug 2023

DOI: https://doi.org/10.22214/ijraset.2023.55484

www.ijraset.com

Call: 08813907089 | E-mail ID: ijraset@gmail.com

International Journal for Research in Applied Science & Engineering Technology (IJRASET)
ISSN: 2321-9653; IC Value: 45.98; SJ Impact Factor: 7.538
Volume 11 Issue VIII Aug 2023- Available at www.ijraset.com

Pushover Analysis of Structures Subjected to Combined Actions of Earthquake and Wind

Mr. Naman Kumar Rai[1], Prof. Anubhav Rai[2]
[1]*P.G. Scholar, Gyan ganga institute of technology and science, Jabalpur, India*
[2]*Professor, Department of Civil Engineering, Gyan ganga institute of technology and science, Jabalpur, India*

***Abstract:** This paper puts forward a framework to investigate the structural performance of buildings subject to the combined action of earthquakes and wind. The study uses a pushover analysis to determine strength capacities of low- and medium-rise concrete structures to compare versus their strength, as inferred from the Indian code for seismic design. The analysis addresses soil-structure interactions through the scrutiny of fixed-base and flexible- base conditions of three soil types ranging between dense and soft. The parametric study covers micro me- topological winds whose mean value spans between 0.5 m/s and 20 m/s. The simulated multi-load scenarios induce ductility levels going from 1 to 6 to totalize 288 case studies. The proposed framework reveals that consideration of earthquake and wind simultaneous effects could modify performance levels used for design through enhancing ductility demands. This evidences that, under current design recommendations, structures located in earthquake prone areas susceptible to unexpected levels of damage.*

I. INTRODUCTION

Composite construction is a generic term to describe any building construction involving multiple dissimilar materials. Composite construction is often used in building aircraft, watercraft, and building construction.

There are several reasons to use composite materials including increased strength, aesthetics, and environmental sustainability. In developing countries like India, most of the building structures fall under the category of low-rise building. So, these conventional Reinforced cement concrete and pure sectional steel construction prove to be convenient and economical in nature hence widely used all around. But when it comes to the need for vertical growth of building due to lack of land space area and rapid growth of population, medium high-rise building emerges as a solution to full - fill this need. The combination of steel and reinforced concrete, thereby utilizing the unique characteristics of the two materials, generally results in structures of greater economy and safety than either material alone could achieve. Because of this, engineers have been continually interested in finding practical and effective ways of joining the materials, in developing new design concepts, and in establishing requirements for satisfactory performance. In the recent years, very significant advances have been made in all these areas, thus leading to a widespread use of combined steel and concrete elements in construction of buildings, bridges, nuclear power plants, and other types of engineering structures. The paper is an attempt to study the behavior of reinforced concrete, steel and composite structure under the effect of seismic loading. The parameters considered are base shear, displacement and story drift.

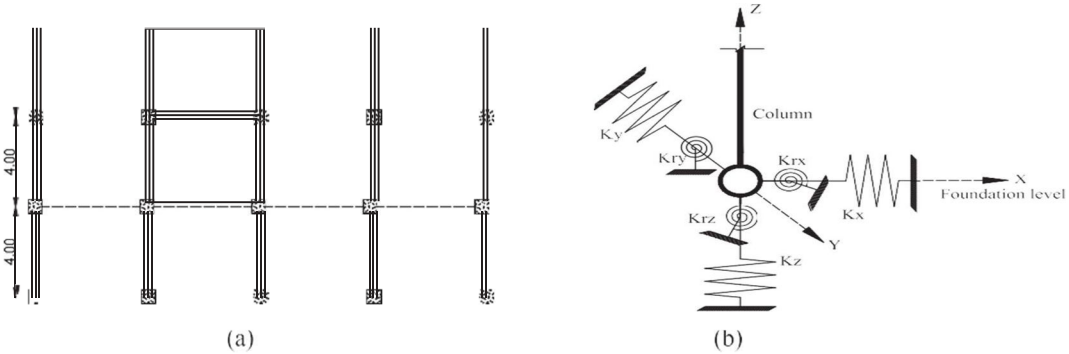

Fig. 1. (a) Plan view of the two structures studied herein; (b) Idealization of foundation system: KX, Ky, Kz, KrX, Kry, Krz are stiffnesses of equivalent soil springs along the translational and rotational degrees of freedom about X, Y and Z axes, respectively.

Table 1
Properties of the three considered soil types adopted in IBC.

Soil type	Soil profile	Range of shear wave velocity, C_s	Average shear wave velocity (m/s)	Poisson's ratio, ν	Initial shear modulus, G_0 (kN/m^2) × 10^3	Effective shear modulus $G = 0.42G_0$ (kN/m^2) × 10^3
A	Very dense soil and soft rock	$360 < C_s < 750$	564	0.25	67.5	28.4
B	Stiff soil	$180 < C_s < 360$	270	0.25	13.7	5.75
C	Soft soil	$C_s < 180$	160	0.25	4.4	1.85

Table 2
Expressions for stiffnesses of equivalent springs along various degrees of freedom as presented elsewhere [26] and used in [23–25].

Degrees of freedom	Stiffness of equivalent soil spring
Vertical	$(\frac{2GL}{1-\nu})[0.73 + 1.54(\frac{A_b}{4L^2})^{0.75}]$
Horizontal (lateral direction)	$(\frac{2GL}{2-\nu})[2 + 2.5(\frac{A_b}{4L^2})^{0.85}]$
Horizontal (longitudinal direction)	$(\frac{2GL}{2-\nu})[2 + 2.5(\frac{A_b}{4L^2})^{0.85}] - (\frac{0.2}{0.75-\nu})GL[1 - (\frac{B}{L})]$
Rocking (about the longitudinal)	$(\frac{G}{1-\nu})I_{bx}^{0.75}(\frac{L}{B})^{0.25}[2.4 + 0.5(\frac{B}{L})]$
Rocking (about the lateral)	$(\frac{3G}{1-\nu})I_{by}^{0.75}(\frac{L}{B})^{0.15}$
Torsion	$3.5GI_{bz}^{0.75}(\frac{B}{L})^{0.4}(\frac{I_{bz}}{B^4})^{0.2}$

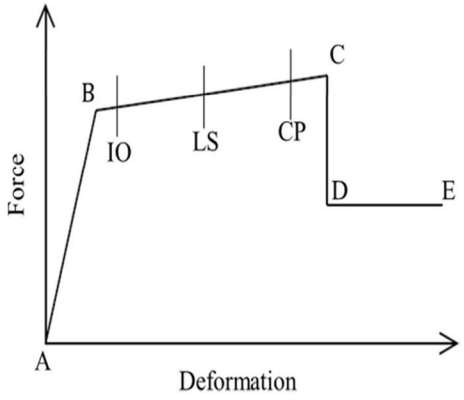

Fig. 2. Force-deformation relationship of a typical plastic mechanism.

II. DESCRIPTION OF STRUCTURAL SYSTEMS

This study considers two reinforced-concrete (RC) structures with 5 and 8 stories, respectively. These are framed with typical beam-column joints without shear walls, and lie in regions with high-seismicity. The buildings were designed for earthquake resistance according to the "Code for Seismic Design of Buildings". Both buildings cover a surface of 16 m by 20 m in plan (Fig. 1(a)) and have a standardized floor-to-floor height of 3 m. The cross section of beams and columns for either structure are 0.5 m × 0.2 m and 0.5 m × 0.5 m, respectively, while slabs have a thickness of 0.15 m. The axial compressive strength f_{ck} of all members is 20 MPa, which is corresponding to the concrete.

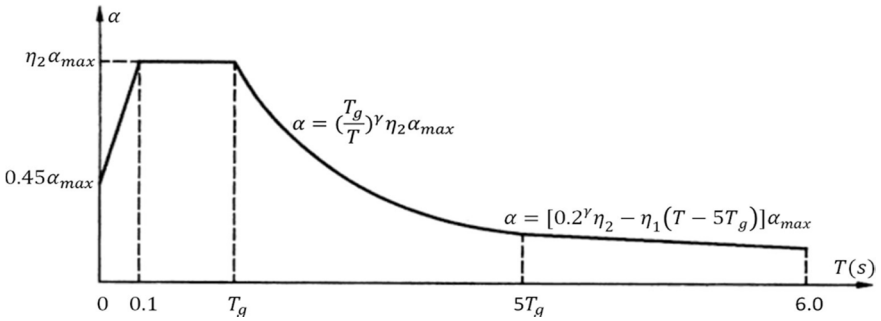

Fig. 3. Seismic influence coefficient curve in the Code.

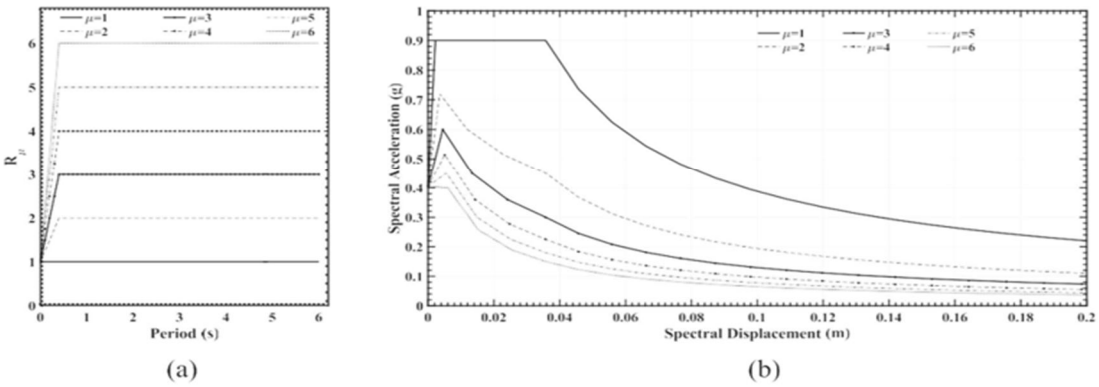

Fig. 4. (a) Rμ-T model (Q-model, mass-proportional damping) proposed by Vidic et al.; (b) Demand spectra of different ductility level μ in ADRS format.

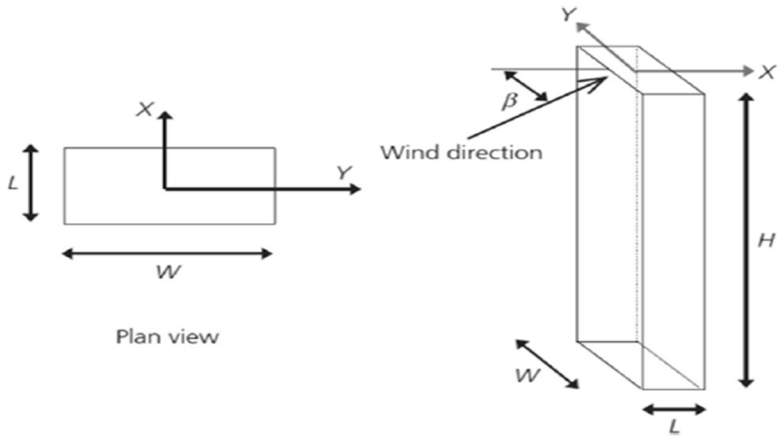

Fig. 5. Geometry of full-scale structures for analysis

Table 3
Derived R^{*}_{μ}/R_{μ} with $\bar{U}$, Γ and μ averaged across $T \leq 2$ s.

		μ					
	$\bar{U}$: m/s	1	2	3	4	5	6
$\Gamma_{5F} = 22.39$	0.5	1.000	0.994	0.969	0.944	0.912	0.917
	5	1.000	0.951	0.935	0.894	0.872	0.836
	10	1.000	0.905	0.852	0.787	0.753	0.721
	15	1.000	0.871	0.783	0.707	0.672	0.633
	20	1.000	0.850	0.766	0.674	0.618	0.562
$\Gamma_{8F} = 28.13$	0.5	1.000	0.991	0.964	0.935	0.898	0.904
	5	1.000	0.956	0.947	0.911	0.892	0.858
	10	1.000	0.919	0.871	0.821	0.787	0.752
	15	1.000	0.893	0.812	0.736	0.704	0.663
	20	1.000	0.872	0.795	0.703	0.647	0.589

grade "C30". The yield and ultimate strengths of longitudinal and transverse rebar were set to be 335 MPa and 455 MPa, respectively. The dead load considered in the analysis included self-weight of structural members, additional 1.7 kN/m^2 due to floor finishes, and 8.5 kN/m acting along each beam to represent light ductile partitions and external facades. The live load was set as 2.0 kN/m^2. All loads are in agreement with the Code provisions. In this study, three-dimensional models of framed structures were modelled for the pushover analysis in SAP2000 version 20 The structural design addressed material properties and load configurations that are relevant to seismic-resisting structures. Beams and columns performed as nonlinear frame elements with lumped plasticity, hence could develop plastic hinges at both ends. We used the default-hinge properties provided by the program and assign the PMM hinges for columns and M3 hinges for beams as recommended. Most design codes characterize soil types based on the shear wave velocity Cs. This study investigates three types of soil, as classified by the IS :1893 PARET I. These are types A, B and C, whose basic properties appear in Table 1. Impedance functions associated with rigid massless foundations controlled the simulated soil- structure interaction whereas the soil physical properties worked as a lumped parameter system at foundation level through them constitute a capacity spectrum. The demand of strength against earth- quake ground motions come from the local elastic response spectra of acceleration. There is also a transformation process here, according to which the diagram showing spectral acceleration versus period be- comes the Acceleration-Displacement Response Spectrum (ADRS). It follows that the intersection of the capacity spectrum and the demand spectrum provides an estimation of the inelastic performance of the structure.

III. CAPACITY CURVE

The pushover analysis, as applied herein, induced a monotonically increasing displacement-controlled lateral load pattern, in the presence of constant gravity load, until an ultimate condition appeared. The applied lateral loads relate to accelerations that the structure would experience during ground shakings. Under incrementally increasing loading, some structural members may yield sequentially. Consequently, parameterization with stiffness coefficients. The stiffness of the idealized springs representing the soil-flexibility are highly sensitive to the size of their footing. Therefore, their dimensions either reflect the ultimate or serviceability limit state, as specified in the relevant Code of Practice. From this derives that the footings underlying each column have dimensions of 4 m × 4 m, and that satisfies all the re- querulents. The three translational springs located at the base of the ground floor columns, two in principal horizontal and one in the vertical di- rection, together with rotational springs about these mutually perpendicular a x e s , simulate soil-flexibility (Fig. 1(b)). The boundary element method and experimental tests were in use to calibrate the properties of springs as these were hypothetically resting on homo- generous elastic half- space. The modelling technique, mapped from Gazeta's and reflected in the set of equations listed in Table 2, is shared practice to dealing with soil-structure interaction - see for ex- ample hence considered suitable for the purpose of this investigation. Its main features account dependability of spring stiffness on mechanical characteristics of the soil material that supports the structure as well as on the dimensions of the foundation. In addition, the mechanical characteristics of t h e foundation soil medium translate into an effective shear modulus G and Poisson's ratio. Here the effective shear modulus G relates to the initial shear modulus go. Although the foundation embedment depth did not influence the estimation of stiffness for springs, it did feed in to computing the bearing capacity of the simulated soil-flexibility. According to Bowles he depth of the foundation has little influence on the bearing capacity of springs; hence its consideration seems confined to cases where controlled construction conditions do exist. As pointed out bent he structural stiffness changes past the yield point, de- noted as B in Fig.2 This figure also illustrates the acceptance criteria as defined by ATC-40. That criterion defines specific performance thresholds such as Immediate Occupancy (IO), Life Safety (LS) and Collapse Prevention (CP), corresponding to 10%, 60%, and 90% of plastic hinge deformation capacity, respectively. Thus, the two in- ventilated structures were subject to gravitational forces and the in- cemental lateral loading. The latter increased step-by-step in the nonlinear static analysis, keeping displacements under control via target tip node displacements of 4% with respect to the total height of the structure, as specified in ATC-40. This process included P-delta effects to defining total forces acting on structural members hence the respective deformations.

A. Seismic Demand of multi-Hazard Scenarios According to STF factor

For an elastic SDOF system the following relation applies:

$$de = \frac{T^2}{4\ 2}\ ae \qquad S = \frac{}{\pi}\ S \qquad (1)$$

where Sae and Sde are values in the elastic spectrum of acceleration and displacement, respectively, corresponding to the period T and a fixed viscous damping ratio. For an inelastic SDOF system with a bilinear force-deformation relationship, the acceleration spectrum (S_a) and displacement spectrum (S_d) can be determined as

$$S_a = \frac{S_{ae}}{R_\mu} \quad (2)$$

fore, the modelling of soil as outlined here enables scrutinizing soil- $S = \frac{\mu}{S} = \frac{\mu}{T^2} S = \mu T^2 S$

Structure interactions on earthquake prone areas underlain by three different soil types. This complements the analysis of fixed-base condition of the subject buildings, for comparison. The fiXed-base dis- regards soil-flexibilities. Bearing in mind that he flexibility of soil causes an overall decrease in lateral stiffness leading to the lengthening of lateral natural periods, we regard the base which considers the soil- flexibility as the flexible-base. The motivation of that parametric study derived from past studies that show how SSI vary displacement and acceleration demands of structures, which contrast with results generated with the fixed-base criteria .

where μ is the ductility factor defined as the ratio between the maximum displacement and the yield displacement. $R\mu$ is the strength re- duction factor, defined as the ratio of the elastic strength demand $Fy(\mu = 1)$ to the inelastic yield strength demand $Fy(\mu t)$ for a given target ductility ratio (μt), which is represented by the following equation:

$$R\mu = Fy(\mu = 1)/Fy(\mu = \mu_t) \quad (4)$$

In this study, the acceleration response spectra S_a (T) was obtained from the "Code for Seismic Design of Buildings", as follows:

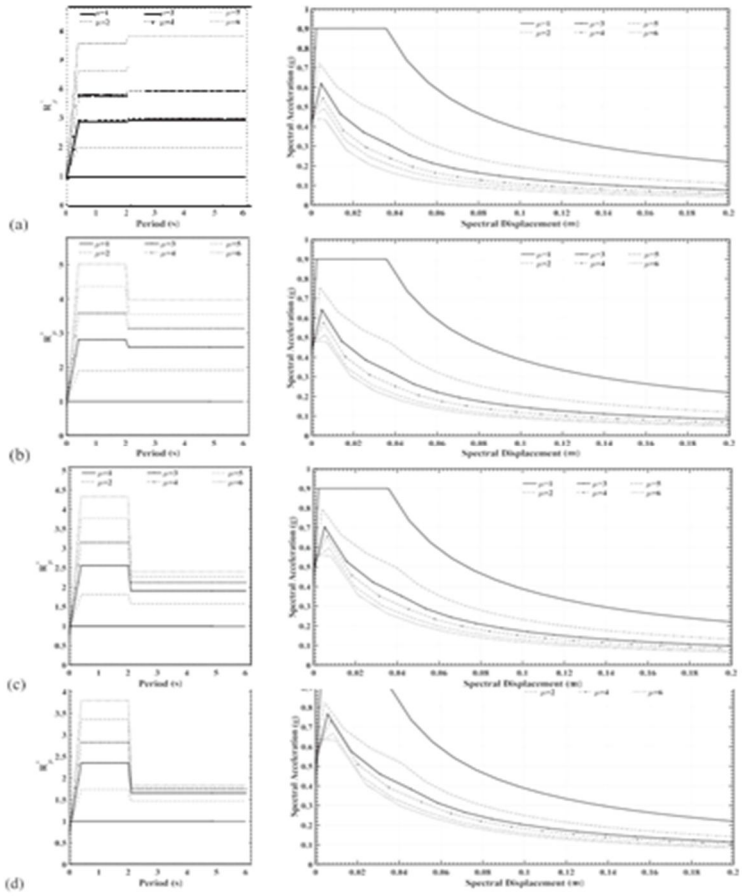

Fig. 6. Deduced R μ -T model and corresponding revised demand spectra of different inelastic level μ for the 5-storey building. (a) $\bar{U}$ =0.5 m/s; (b) $\bar{U}$ =5 m/s; (c) $\bar{U}$ =10 m/s; (d) $\bar{U}$ =15 m/s; (e) $\bar{U}$ =20 m/s.

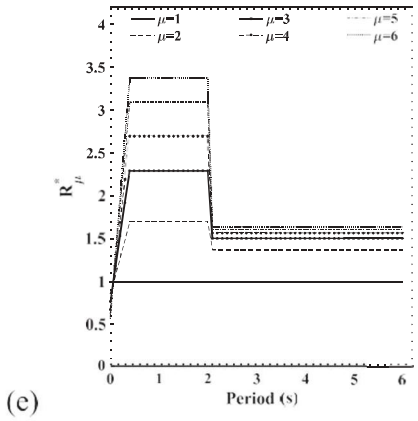

(e)

Fig. 6. (*continued*)

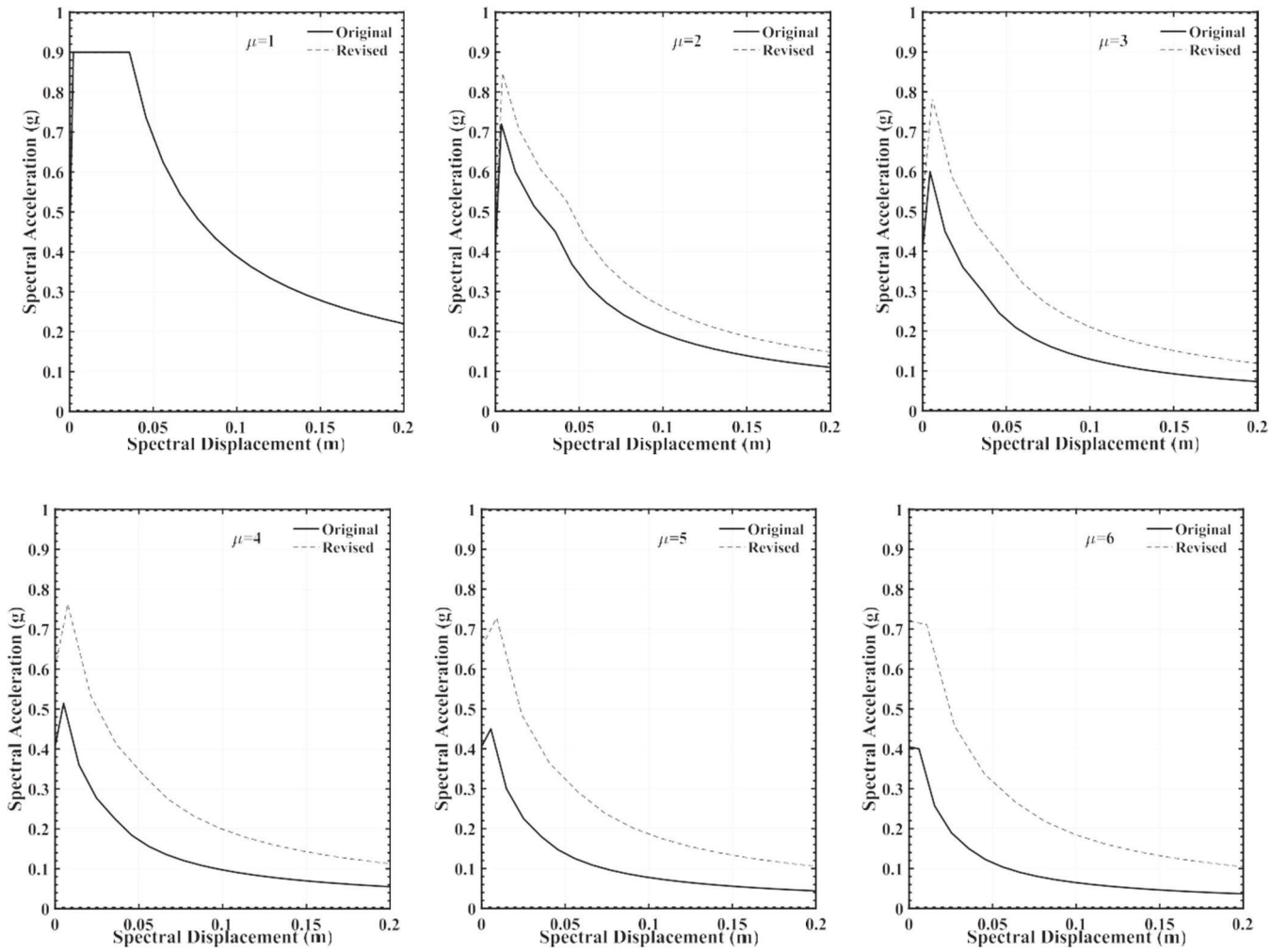

Fig. 7. Comparison of the original and revised demand spectra of different inelastic level μ for the 5-storey building ($\bar{U}$ = 20 m/s).

section, γ = 0.9 + (0.05 – ξ)/(0.5 ≤ 5ξ); - damping ratio; 1- adjustment coefficient for the descending slope in the linear decreasing region,

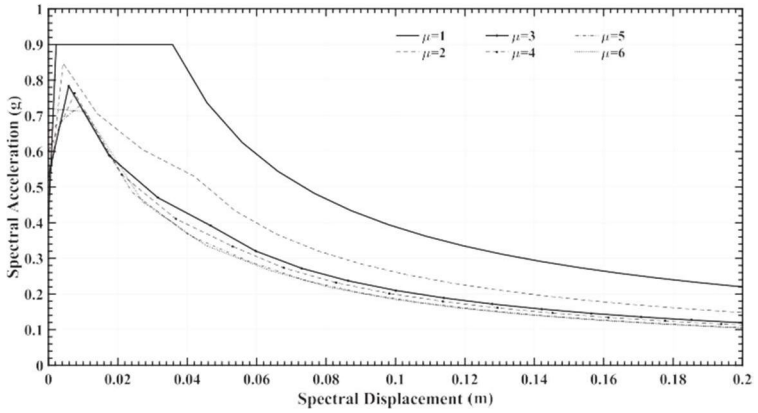

η Code is the acceleration index under the η site class of category II) and "group 2" (which stands for intermediate distance earthquakes). Th is 1 = 0.02 + (0.05)/8, and if 1 < 0, set 1 = 0; 2- damping adjust- defined the value of Tg as 0.40 s. The maximum value of seismic in meant coefficient, 2 = 1 + (0.05)/(0.06 + 1.7); T- period of the fluence coefficient max was set as 0.9 g, corresponding to rare earth-structure; Tg- characteristic period. The curve defining the seismic in- fluence coefficient is shown in Fig. 3.

A constant damping ratio of 5% was set for the acceleration response spectra. The value of the characteristic period Tg depends on the site class and design earthquake group, which were set as "category II" (the basic seismic precautionary criterion specified in the quake occurrence in areas of intensity 8.

According to Vidic et al. and Fajfar Rμ is a function of structural period, target ductility, and characteristic parameters of the relevant hysteretic model. In this study, the Rμ-T model introduced by Vidic et al. was adopted hence the value of Rμ was approximated with a bilinear curve:

Table 7
Top displacements, D and base shear, V at the performance point for the 5-storey building.

U : m/s		FiXed-base		Soil A		Soil B		Soil C	
		D (m)	V (kN)	D (m)	V (kN)	D (m)	V (kN)	D (m)	V (kN)
0	Rμ=1	0.054	3090.559	0.057	3102.572	0.066	3194.387	0.095	3494.404
	Rμ=2	0.024	2267.470	0.026	2262.466	0.032	2233.070	0.046	1944.033
	Rμ=3	0.016	1739.251	0.017	1752.036	0.022	1704.224	0.029	1234.439
	Rμ=4	0.012	1391.398	0.013	1368.410	0.016	1274.779	0.021	905.610
	Rμ=5	0.010	1179.780	0.010	1137.715	0.013	1024.876	0.017	716.414
	Rμ=6	0.008	1037.948	0.009	984.251	0.010	861.292	0.014	592.395
0.5	R μ=1	0.054	3086.243	0.057	3098.634	0.066	3188.582	0.095	3491.417
	R μ=2	0.025	2276.577	0.026	2271.487	0.032	2241.933	0.046	1958.826
	R μ=3	0.017	1783.110	0.018	1800.796	0.022	1759.873	0.030	1276.883
	R μ=4	0.013	1453.737	0.014	1436.726	0.017	1350.119	0.023	963.217
	R μ=5	0.011	1262.125	0.011	1227.207	0.014	1121.114	0.018	788.747

	R μ=6	0.009	1102.339	0.010	1053.809	0.011	935.202	0.015	648.392
5	R μ=1	0.054	3086.243	0.057	3098.634	0.066	3188.582	0.095	3491.417
	R μ=2	0.026	2339.676	0.027	2334.073	0.034	2303.291	0.049	2060.282
	R μ=3	0.017	1835.892	0.019	1859.622	0.023	1827.645	0.031	1329.347
	R μ=4	0.014	1515.757	0.015	1504.943	0.018	1426.003	0.024	1020.802
	R μ=5	0.011	1303.985	0.012	1272.854	0.015	1170.671	0.019	826.392
	R μ=6	0.010	1176.687	0.010	1134.407	0.013	1021.206	0.017	713.206
10	R μ=1	0.054	3086.243	0.057	3098.634	0.066	3188.582	0.095	3491.417
	R μ=2	0.027	2415.752	0.029	2409.212	0.035	2376.495	0.051	2184.237
	R μ=3	0.019	1965.094	0.020	1959.085	0.025	1931.363	0.035	1472.796
	R μ=4	0.015	1674.368	0.017	1680.040	0.020	1622.198	0.028	1171.243
	R μ=5	0.013	1456.962	0.014	1440.347	0.017	1354.216	0.023	966.001
	R μ=6	0.011	1311.794	0.012	1281.415	0.015	1179.772	0.020	833.316
15	R μ=1	0.054	3086.243	0.057	3098.634	0.066	3188.582	0.095	3491.417
	R μ=2	0.028	2465.851	0.030	2458.479	0.036	2424.277	0.053	2266.510
	R μ=3	0.021	2060.303	0.022	2055.188	0.028	2027.634	0.038	1618.539
	R μ=4	0.017	1824.098	0.018	1846.463	0.023	1812.372	0.031	1317.453
	R μ=5	0.015	1590.096	0.016	1586.878	0.019	1517.45	0.026	1090.927
	R μ=6	0.013	1448.063	0.014	1430.449	0.017	1342.927	0.022	957.581
20	R μ=1	0.054	3086.243	0.057	3098.634	0.066	3188.582	0.095	3491.417
	R μ=2	0.029	2502.224	0.031	2509.887	0.037	2473.979	0.055	2352.928
	R μ=3	0.021	2108.201	0.023	2082.443	0.028	2054.816	0.039	1660.445
	R μ=4	0.018	1894.147	0.019	1902.254	0.024	1873.764	0.033	1387.916
	R μ=5	0.016	1699.211	0.017	1707.536	0.021	1653.169	0.028	1195.125
	R μ=6	0.014	1585.641	0.015	1581.901	0.019	1511.706	0.026	1086.664

$$R = c(\mu - 1)^{CR}\frac{T}{T_0} + 1 \quad T \le T_0 \qquad (9)$$

distributed mass (M) while defining a mass to volume ratio parameter
( ). The generalized mass (M*) can be calculated using equation (12):

$$R = c_1(\mu - 1)^{c_R} + 1 \quad T_0 > T \qquad (10)$$

$$M^* = \frac{H^2}{\int_0^{\phi}} \phi(z)\, M(z)\, dz \qquad (12)$$

where T0 is the period dividing the period range into two portions. T0 is related to the predominant period of the ground motion Tg by means of:

where M(z) represents the structural mass per unit length, z is a vertical

$$T_0 = c_2 \mu^{c_T} T_g \qquad (11)$$

coordinate and ϕ is the fundamental modal shape, which was approximate by $\phi(z) = (Z/H)^{\beta}$ where $\beta = 1.5$ and H is the height of the Γ^*

The coefficients c1, c2, cR and cT depend on the assumed hysteretic behavior and damping. The Q-model (mass-proportional damping) was adopted here, therefore according to it c1, c2, cR and cT equal to 1.0, 1.0, 0.65 and 0.30, respectively. The Rμ-T model is shown in Fig. 4(a). In this process, we regard the same strength reduction factor Rμ for the selected support conditions of the buildings namely, fixed-base and flexible-base, which obeys the SSI regulations in the current seismic design codes (ASCE [5]). In other words, it was assumed that SSI has a similar impact on the strength demand of either elastic or inelastic building. The geometries of the prototype building are shown in Fig. 5. This model essentially defines generalized MDOF systems that preserve their volume. The purpose of this is to use the model to quantify the inelastic performance of structures subject to earthquake and wind combined load. The method is analogous to standard techniques used in earthquake engineering to monitoring the inelastic performance of single oscillators leading to determine SRFs. To that end, Martinez- Vazquez defined the mass to volume ratio = $M / (H^2 + W^2 + L^2)^{1/2}$ to characterizing buildings. In the present investigation, took values of structures. Starting from the typical elastic design spectrum according 5F = 22.39 ton/m and 8F = 28.13 ton/m for the two investigated to the Code (equations (5)–(8)), and by using equations (2), (3), (9)– (11), the corresponding demand spectra for the different ductility. factors μ in ADRS format were obtained (Fig. 4(b)).

Table 6

Top displacements, D and base shear, V at the performance point for the 8-storey building.

$\bar{U}$: m/s		Fixed-base		Soil A		Soil B		Soil C	
		D (m)	V (kN)	D (m)	V (kN)	D (m)	V(kN)	D (m)	V (kN)
0	Rμ=1	0.095	3210.033	0.100	3231.834	0.116	3281.823	0.172	3611.394
	Rμ=2	0.042	2110.619	0.046	2111.006	0.057	2148.579	0.080	1845.563
	Rμ=3	0.027	1639.075	0.030	1638.572	0.039	1691.939	0.050	1170.261
	Rμ=4	0.020	1416.417	0.022	1411.233	0.028	1299.775	0.037	858.573
	Rμ=5	0.016	1189.947	0.018	1169.941	0.022	1027.504	0.029	679.379
	Rμ=6	0.014	1029.361	0.015	994.200	0.018	851.582	0.024	563.449
0.5	Rμ=1	0.095	3210.033	0.100	3231.834	0.116	3281.823	0.172	3611.394
	Rμ=2	0.043	2123.612	0.046	2123.846	0.058	2160.453	0.081	1864.604
	Rμ=3	0.028	1672.605	0.031	1672.543	0.040	1726.098	0.053	1217.908
	Rμ=4	0.022	1462.204	0.024	1458.296	0.031	1397.876	0.040	922.095
	Rμ=5	0.018	1297.040	0.020	1288.595	0.025	1150.051	0.033	760.020
	Rμ=6	0.015	1114.872	0.016	1087.273	0.020	943.999	0.027	624.634

5	R μ=1	0.095	3210.036	0.100	3231.834	0.116	3281.823	0.172	3611.394
	R μ=2	0.045	2178.293	0.048	2177.767	0.060	2210.315	0.084	1944.094
	R μ=3	0.029	1689.593	0.031	1689.714	0.041	1743.001	0.054	1241.578
	R μ=4	0.022	1480.931	0.024	1477.446	0.032	1438.151	0.041	948.473
	R μ=5	0.018	1303.902	0.020	1296.169	0.025	1157.328	0.033	765.337
	R μ=6	0.016	1162.088	0.017	1139.261	0.022	996.131	0.028	658.918
10	R μ=1	0.095	3210.036	0.100	3231.834	0.116	3281.823	0.172	3611.394
	R μ=2	0.047	2241.765	0.050	2240.241	0.062	2267.741	0.088	2037.178
	R μ=3	0.032	1774.964	0.034	1775.973	0.044	1828.123	0.059	1362.320
	R μ=4	0.025	1561.086	0.027	1559.307	0.035	1610.328	0.046	1060.759
	R μ=5	0.021	1427.257	0.023	1422.416	0.029	1323.445	0.038	873.788
	R μ=6	0.018	1292.061	0.020	1283.056	0.025	1143.560	0.032	756.547
15	R μ=1	0.095	3210.036	0.100	3231.834	0.116	3281.823	0.172	3611.394
	R μ=2	0.048	2290.128	0.051	2287.756	0.064	2311.262	0.091	2108.728
	R μ=3	0.034	1852.372	0.037	1853.726	0.047	1904.000	0.064	1473.136
	R μ=4	0.028	1656.105	0.030	1655.815	0.039	1709.331	0.051	1193.908
	R μ=5	0.023	1506.798	0.025	1503.874	0.033	1493.212	0.042	984.367
	R μ=6	0.020	1420.146	0.022	1415.205	0.029	1308.366	0.037	863.657
20	R μ=1	0.095	3210.036	0.100	3231.834	0.116	3281.823	0.172	3611.394
	R μ=2	0.050	2330.047	0.053	2326.769	0.065	2346.335	0.094	2167.305
	R μ=3	0.035	1877.194	0.038	1878.592	0.048	1928.169	0.065	1508.877
	R μ=4	0.029	1699.301	0.032	1699.581	0.041	1752.897	0.054	1255.294
	R μ=5	0.025	1573.372	0.028	1571.808	0.036	1624.668	0.046	1077.605
	R μ=6	0.023	1502.966	0.025	1499.992	0.033	1485.720	0.042	979.212

required interpolating the curves given in using the Lagrange In- trepidation Polynomial method, with respect to the mass to volume ratio 5F and 8F that characterize our target buildings. The resulting values of R μ/Rμ, once averaged over the ranges T 2 s and T>2 s for the 5-storey and 8-storey buildings are listed in Table 3 and Table 4, re- sportively. The criterion of sub-dividing the interval of 0.1s T 5s specified for SRFs in reflects the fact that the original curves show different steadiness past T = 2 s. It follows that a revised demand spectra associated to different inelastic levels μ can be produced, now using the SRFs related to multi-hazards conditions. Fig. 6 shows the deduced R μ-T model for the 5-storey building for when 0.5 m/s $\bar{U}$ 20 m/s. In addition, Fig. 7 compares the original and revised demand spectra for different inelastic level μ for the 5-storey building subject to a wind velocity of $\bar{U}$ = 20 m/s. Following the procedure detailed above, we deduced the R μ-T model for the 8-storey building reaching different inelastic levels μ and subject to different wind velocities $\bar{U}$. The results showed similar trends than those illustrated in Fig. 6, hence those not presented here for brevity. In general, the results obtained show that the amplitude and shape of the R μ -T curves depend on the wind velocity $\bar{U}$ and the ratio of mass to volume Γ. The observed decrease of R μ/Rμ fluctuated between 20 and 60%, including low wind level scenarios, but go below these limits with increased average wind speed.

IV. PUSHOVER ANALYSIS RESULTS

The results presented above enable comparing strength demands for the two buildings, associated to various ductility levels. Based on the pushover analysis performed with SAP2000, a capacity curve of the structure was generated (roof displacement verses the base shear) for each load case. For the sake of clarity, the identified intersection be- tween the capacity and demand curves appear in Table 5 and Table 6. These Tables primarily show that for all systems to maintaining target ductility levels the displacement and force demands increase gradually with the wind velocity. Evidently, strength demands in any form reduce inversely proportional to the ductility μ.

ISSN: 2321-9653; IC Value: 45.98; SJ Impact Factor: 7.538
Volume 11 Issue VIII Aug 2023- Available at www.ijraset.com

The capacity curves shown in Fig. 8 and Fig. 9 illustrate performance levels for investigated different wind speeds $\bar{U}$ and support conditions, related to the 5-storey and 8-storey buildings, respectively. The solid line stands for the capacity curve derived from the fixed-base condition while the dashed line stands for the capacity derived from using soil type C; the discrete symbols correspond to performance points: circles are for μ = 1, squares are for μ = 3 and triangles are for μ = 6; black markers represent the action of single earthquakes and the red ones represent the combined action of earthquakes and wind. Two curves are included in these figures to represent the fixed-base case and most flexible-base case, correspondingly. The ordinated of the estimated performance point stress the fact that the higher the wind

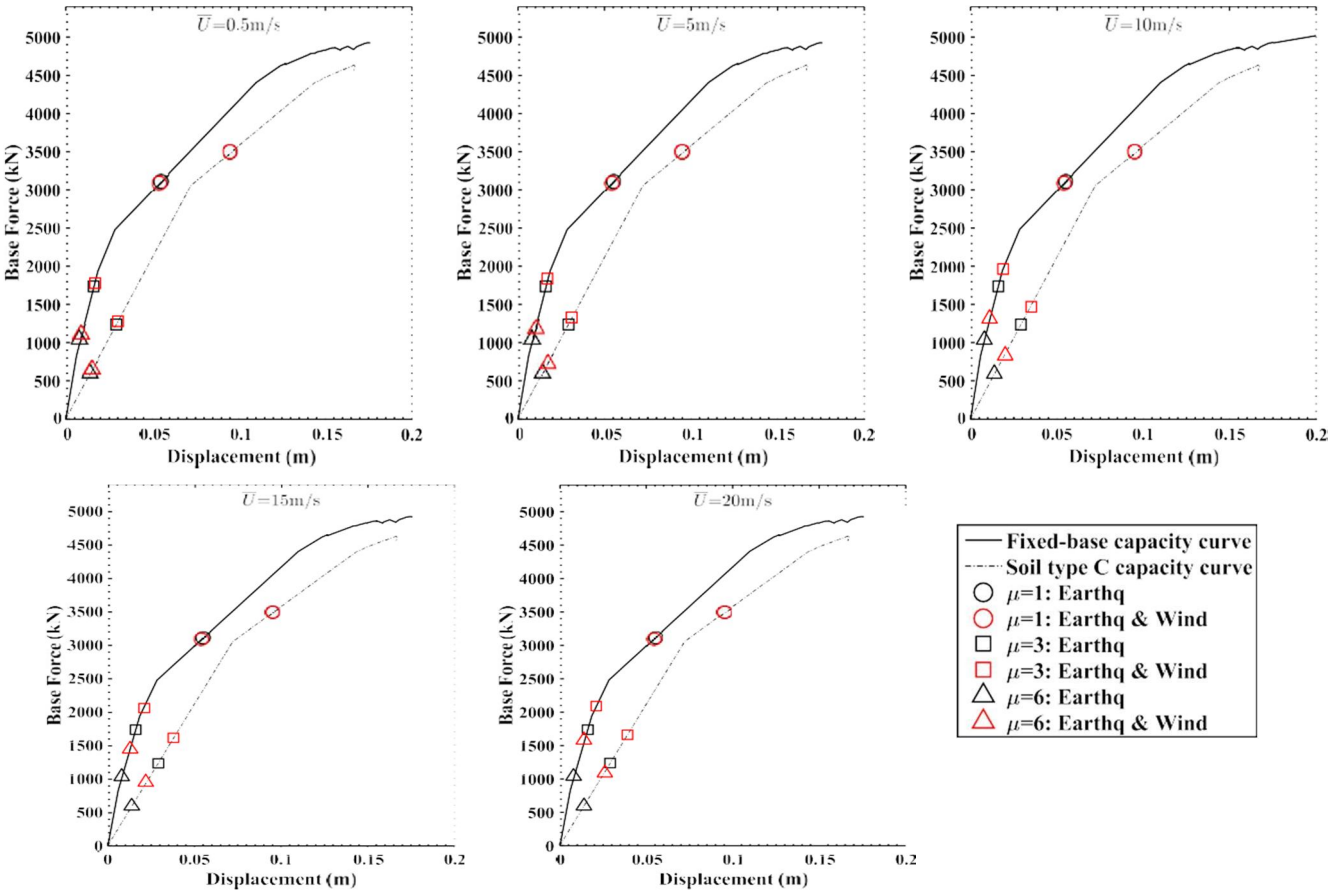

Fig. 8. Capacity curves and performance points associated to different inelastic levels μ and wind speeds $\bar{U}$ for the 5-storey building.

velocity or inelastic level is, the larger the difference between the strength demands associated to earthquake and wind joint events and earthquake forces acting alone.

To draw more general conclusions, the rate of variation in base shear and roof displacement due to earthquake and wind joint effects were investigated. This involved both, the 5-storey and 8-storey buildings with consideration of soil-structure interaction. The corresponding results are shown in Tables 7–10, which highlight the potential impact of multi-hazard events on buildings. These results re- iterate that strength and displacement demands would increase with wind speed and inelastic levels at the time that dimension Alise the change. In light of these results, the impact of wind speed $\bar{U}$ on the value of performance points seem remarkable. The rate of increase of both force and displacement demands is considerable even for low values of $\bar{U}$· see Table 7, shows that the force re-quired to maintain target ductility values is of 0.4%, 2.52%, 4.48%, 6.98% and 6.2% for μ equal to 2, 3, 4, 5 and 6 respectively. Further- more, the increased rate in displacement demand shown in Table 9 is even higher: 4.17%, 6.25%, 8.33%, 10% and 12.5% corresponding to6μ = 2–6, respectively. Generally, the highest changes would occur within the intervals of 0.5 m/s ≤ $\bar{U}$ ≤ 10 m/s regardless of the structural heights and support conditions.

To better visualize the above results, Fig. 10 and Fig. 11 were plotted based on Table 7–8 and Table 9–10, respectively. With respect to force capacity demands derived from analyzing multi-hazard conditions, Fig. 10 shows that the rate of change in the base shear due to the in- creased wind velocity is higher for systems with a more pronounced

For example, the capacity demand of 5-storey building with fixed- base associated to $\bar{U}$ = 0.5 m/s, soil-structure interaction. As for the 5-storey building, for instance, the ratio of Rate of change (%) in force capacity demand between the most flexible-base and the fixed-base structure for each ductility level was calculated, which gives an averaged ratio as approximately 1.55. Specifically, when the wind velocity reaches $\bar{U}$ = 20 m/s and the in-elastic level μ is at the highest value of 6, the rate of change associate to the force capacity demand for the fixed-base subject to multi-hazard conditions is about 45% higher than that under single earthquake activity. The same parameter exhibits a gradually trend of increase with decreasing hardness of soil. That increase is roughly 50%, 60% and 70% for soil type A, B and C, respectively. The increase of force capacity demand for the 8-storey building is similar, although, the magnification of the overall rate of change is slightly lower, accounting for about 0.85 to 0.9 of the 5-storey building, for each support condition. The results presented in the form of percentage of the rate of change increase in base shear due to the soil-flexibility highlights the significance of con- side ring this soil-structure interaction in structural analysis.

As for roof displacement capacity demands, the results indicate that multi-hazard load scenarios can also have significant impact. A com- parison against equivalent rate of change in force capacity demands, show an increase of displacement demands for both buildings that could reach up to 60% when μ= 6 and $\bar{U}$ = 20 m/s, for all soil types and including the fixed-base condition. It is to note however, that there is not substantial difference of such magnification of capacity demand between the fixed-base and flexible-base support conditions. This trend is also observed in Fig. 11, related to floor displacement demand for both the 5-storey and 8-storey building. In that case, the increase in threat of change for flexible supports is of around 60–70% in the worst possible scenario. In general, the results obtained show little variation

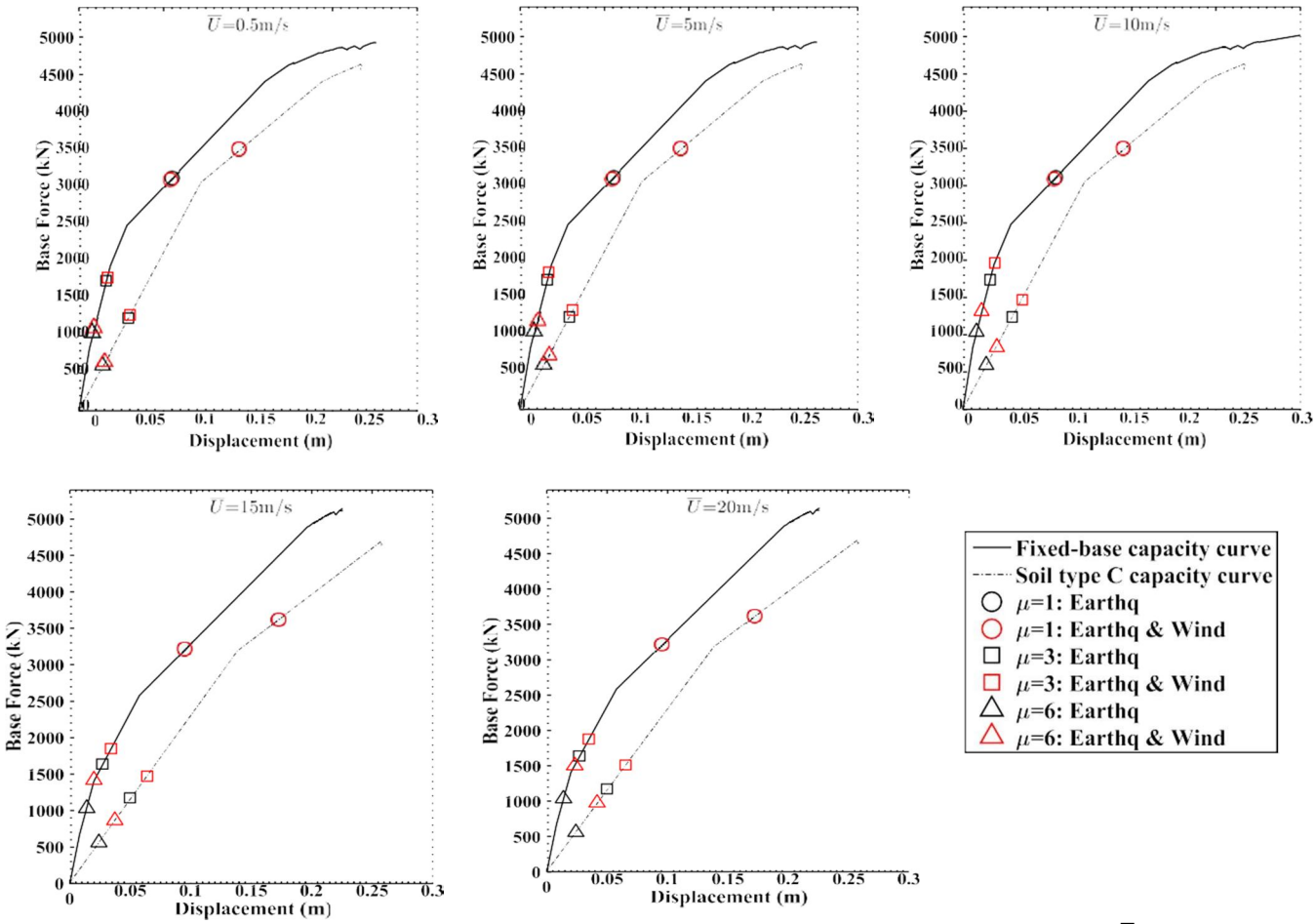

Fig. 9. Capacity curves and performance points associated to different inelastic levels μ and wind speeds $\bar{U}$ for the 8-storey building.

for the low- and medium-rise buildings. A potential explanation of this relates to the observed proportionality between the ratio R_μ/R_μ and the structural mass to volume ratio Γ, i.e. the higher the value of Γ the larger the SRF associated to multi-hazard conditions R_μ. In this in-dimensional finite element method. The latter involving three soil types ranging between dense and soft, hence addressing the impact of soil- structure interaction. The averaged wind velocity $\bar{U}$ varied between 0.5 m/s and 20 m/s while target ductility levels μvaried between1 and ventilation we obtained 5F = 22.39 ton/m, 8F = 28.13 ton/m, which 6, to totalize 288 case studies.

The investigation revealed significant implies that the 8-storey building would have a higher SRF R_μ than the 5- storey building. This derived in a lower demand of strength to withstand earthquake and wind joint load with respect to that associated to the single earthquake condition that would balance the re- lative differences between capacity and demand for the two case studies. The observed proportionality between R_μ and Γ also suggests that those structures with relatively low Γ are more susceptible to exceed target performance demand levels than relatively large (massive) structures if these were designed with SRFs corresponding to the zero-wind load condition.

V. DISCUSSION AND CONCLUSIONS

The paper puts forward a framework to investigate structural performance under the combined action of earthquakes and wind. The procedure involves pushover analysis to determine structural strength. variability of structural performance due to the earthquake and wind joint effects, with respect to current design approaches solely based on earthquake loading. The proposed method could inform further studies on seismic vulnerability for structures subject to multi-hazard sce- narios.

The current seismic design codes recommend the same strength reduction factors for both fiXed-base and flexible-base structures (eg, ASCE [5]). This consideration implicitly assume that the reduction of design base shear for both elastic and inelastic building performance is proportional. However, the results obtained suggest that of the impact of SSI on inelastic performance is not as clear as it is for elastic per- formance. In other words, the lack of distinction amongst the referred support conditions, as reflected in the code recommendations, would cause excessive reduction of the yield strength for the flexible-base structures, and in turn, lead to higher displacement demands in the flexible-base structure compared with the fiXed-base structure. These findings are illustrated in Table 5 and Table 6, which also show that displacement demands in flexible-base structures exceed those of fiXed-base structures analysed by using the same strength reduction factor considering fiXed-base and flexible-base conditions using three-

Table 9

Rate of change (%) in roof displacement for the 5-storey building related to different wind velocity intervals.

	Deviation %	$\bar{U}_{0.5}$ / $\bar{U}_0$	$\bar{U}_5$ / $\bar{U}_{0.5}$	$\bar{U}_{10}$ / $\bar{U}_5$	$\bar{U}_{15}$ / $\bar{U}_{10}$	$\bar{U}_{20}$ / $\bar{U}_{15}$
FiXed-base	R_μ=1	0.00	0.00	0.00	0.00	0.00
	R_μ=2	0.40	2.77	3.25	2.07	1.48
	R_μ=3	2.52	2.96	7.04	4.85	2.32
	R_μ=4	4.48	4.27	10.46	8.94	3.84
	R_μ=5	6.98	3.32	11.73	9.14	6.86
	R_μ=6	6.20	6.74	11.48	10.39	9.50
Soil A	R_μ=1	0.00	0.00	0.00	0.00	0.00
	R_μ=2	0.40	2.76	3.22	2.04	2.09
	R_μ=3	2.78	3.27	5.35	4.91	1.33
	R_μ=4	4.99	4.75	11.63	9.91	3.02

	Deviation %	$\bar{U}_{0.5}$ / $\bar{U}_0$	$\bar{U}_5$ / $\bar{U}_{0.5}$	$\bar{U}_{10}$ / $\bar{U}_5$	$\bar{U}_{15}$ / $\bar{U}_{10}$	$\bar{U}_{20}$ / $\bar{U}_{15}$
FiXed-base	R_μ=1	0.00	0.00	0.00	0.00	0.00
	R_μ=2	4.17	4.00	3.85	3.70	3.57
	R_μ=3	6.25	0.00	11.76	10.53	0.00
	R_μ=4	8.33	7.69	7.14	13.33	5.88
	R_μ=5	10.00	0.00	18.18	15.38	6.67
	R_μ=6	12.50	11.11	10.00	18.18	7.69
Soil A	R_μ=1	0.00	0.00	0.00	0.00	0.00
	R_μ=2	0.00	3.85	7.41	3.45	3.33
	R_μ=3	5.88	5.56	5.26	10.00	4.55
	R_μ=4	7.69	7.14	13.33	5.88	5.56

	R μ=5	7.87	3.72	13.16	10.17	7.60
	R μ=6	7.07	7.65	12.96	11.63	10.59
Soil B	R μ=1	0.00	0.00	0.00	0.00	0.00
	R μ=2	0.40	2.74	3.18	2.01	2.05
	R μ=3	3.27	3.85	5.67	4.98	1.34
	R μ=4	5.91	5.62	13.76	11.72	3.39
	R μ=5	9.39	4.42	15.68	12.05	8.94
	R μ=6	8.58	9.20	15.53	13.83	12.57
Soil C	R μ=1	0.00	0.00	0.00	0.00	0.00
	R μ=2	0.76	5.18	6.02	3.77	3.81
	R μ=3	3.44	4.11	10.79	9.90	2.59
	R μ=4	6.36	5.98	14.74	12.48	5.35
	R μ=5	10.10	4.77	16.89	12.93	9.55
	R μ=6	9.45	10.00	16.84	14.91	13.48

	R μ=5	10.00	9.09	16.67	14.29	6.25
	R μ=6	11.11	0.00	20.00	16.67	7.14
Soil B	R μ=1	0.00	0.00	0.00	0.00	0.00
	R μ=2	0.00	6.25	2.94	2.86	2.78
	R μ=3	0.00	4.55	8.70	12.00	0.00
	R μ=4	6.25	5.88	11.11	15.00	4.35
	R μ=5	7.69	7.14	13.33	11.76	10.53
	R μ=6	10.00	18.18	15.38	13.33	11.76
Soil C	R μ=1	0.00	0.00	0.00	0.00	0.00
	R μ=2	0.00	6.52	4.08	3.92	3.77
	R μ=3	3.45	3.33	12.90	8.57	2.63
	R μ=4	9.52	4.35	16.67	10.71	6.45
	R μ=5	5.88	5.56	21.05	13.04	7.69
	R μ=6	7.14	13.33	17.65	10.00	18.18

Table 10

Rate of change (%) in roof displacement for the 8-storey building related to different wind velocity intervals.

	Deviation %	Δ U 0.5 / U 0	Δ U 5 / U 0.5	Δ U 10 / U 5	Δ U 15 / U 10	Δ U 20 / U 15
FiXed-base	R μ=1	0.00	0.00	0.00	0.00	0.00
	R μ=2	0.62	2.57	2.91	2.16	1.74
	R μ=3	2.05	1.02	5.05	4.36	1.34
	R μ=4	3.23	1.28	5.41	6.09	2.61
	R μ=5	9.00	0.53	9.46	5.57	4.42
	R μ=6	8.31	4.24	11.18	9.91	5.83
Soil A	R μ=1	0.00	0.00	0.00	0.00	0.00
	R μ=2	0.61	2.54	2.87	2.12	1.71
	R μ=3	2.07	1.03	5.10	4.38	1.34
	R μ=4	3.33	1.31	5.54	6.19	2.64
	R μ=5	10.14	0.59	9.74	5.73	4.52
	R μ=6	9.36	4.78	12.62	10.30	5.99
Soil B	R μ=1	0.00	0.00	0.00	0.00	0.00
	R μ=2	0.55	2.31	2.60	1.92	1.52
	R μ=3	2.02	0.98	4.88	4.15	1.27
	R μ=4	7.55	2.88	11.97	6.15	2.55
	R μ=5	11.93	0.63	14.35	12.83	8.80

	Deviation %	Δ U 0.5 / U 0	Δ U 5 / U 0.5	Δ U 10 / U 5	Δ U 15 / U 10	Δ U 20 / U 15
FiXed-base	R μ=1	0.00	0.00	0.00	0.00	0.00
	R μ=2	2.38	4.65	4.44	2.13	4.17
	R μ=3	3.70	3.57	10.34	6.25	2.94
	R μ=4	10.00	0.00	13.64	12.00	3.57
	R μ=5	12.50	0.00	16.67	9.52	8.70
	R μ=6	7.14	6.67	12.50	11.11	15.00
Soil A	R μ=1	0.00	0.00	0.00	0.00	0.00
	R μ=2	0.00	4.35	4.17	2.00	3.92
	R μ=3	3.33	0.00	9.68	8.82	2.70
	R μ=4	9.09	0.00	12.50	11.11	6.67
	R μ=5	11.11	0.00	15.00	8.70	12.00
	R μ=6	6.67	6.25	17.65	10.00	13.64
Soil B	R μ=1	0.00	0.00	0.00	0.00	0.00
	R μ=2	1.75	3.45	3.33	3.23	1.56
	R μ=3	2.56	2.50	7.32	6.82	2.13
	R μ=4	10.71	3.23	9.38	11.43	5.13
	R μ=5	13.64	0.00	16.00	13.79	9.09

Soil C	R_{*} μ=6	10.85	5.52	14.80	14.41	13.56
	R_{*} μ=1	0.00	0.00	0.00	0.00	0.00
	R_{*} μ=2	1.03	4.26	4.79	3.51	2.78
	R_{*} μ=3	4.07	1.94	9.72	8.13	2.43
	R_{*} μ=4	7.40	2.86	11.84	12.55	5.14
	R_{*} μ=5	11.87	0.70	14.17	12.66	9.47
	R_{*} μ=6	10.86	5.49	14.82	14.16	13.38

Soil C	R_{*} μ=6	11.11	10.00	13.64	16.00	13.79
	R_{*} μ=1	0.00	0.00	0.00	0.00	0.00
	R_{*} μ=2	1.25	3.70	4.76	3.41	3.30
	R_{*} μ=3	6.00	1.89	9.26	8.47	1.56
	R_{*} μ=4	8.11	2.50	12.20	10.87	5.88
	R_{*} μ=5	13.79	0.00	15.15	10.53	9.52
	R_{*} μ=6	12.50	3.70	14.29	15.63	13.51

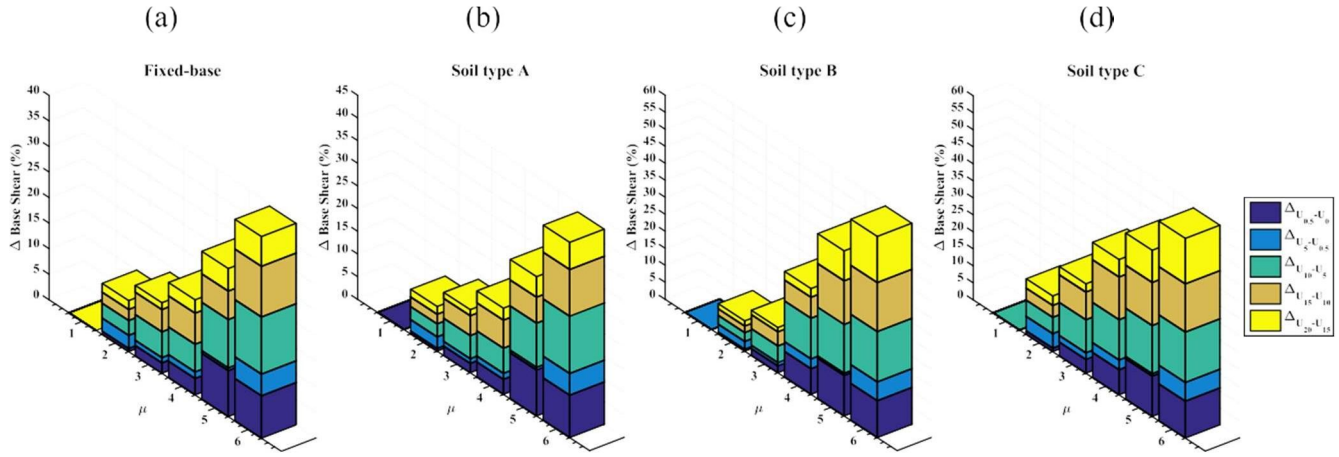

Fig. 10. Rate of change (%) in base shear related to wind velocity intervals. (a)-(d) results of the 5-storey and (e)-(h) results of the 8-storey building with fiXed-base and soil types A to C.

(while of the opposite is true when looking at results involving force demands). Furthermore, the rate of force demand for flexible-base structures increases with the wind speed at higher rates than it does for fiXed-base structures.

The analysis of the probabilities of wind occurrence in normal conditions reported in suggests that in certain regions wind velo- cities of 5 m/s are susceptible to be exceeded in up to 75% of time,

whereas those within the range of 5 m/s $< \bar{U} <$ 10 m/s can be exceeded 25% of time. It therefore seems non-conservative to ignore the potential occurrence of earthquake and wind joint events during the design stage. The criteria reflected in current codes of practice assume that return periods associated to joint events exceed those related to single load action, however such considerations ignore that the return period of ground motions is not fiXed and can vary significantly from one area to another. In NOAA is shown that the number of earthquakes with magnitude above 6.5 recorded in the last 50 years totalise 789, whereas 118 and 18 of those events have occurred within the last 5 years and during 2018, respectively. This combined with the number of recorded aftershocks that follow major earthquake events make infrastructure susceptible to multi-hazard scenarios induced by earthquakes and wind, both during construction and once in operation. This is a permanent risk that to date remains unquantified. The pro- posed framework recognises that integrating wind actions on earth- quake resisting design procedures would enable mitigating such risk, particularly when such approach takes into account seismic re- gionalisation. In that context, it is recommended that an integrated risk analysis considers the variation of wind regimes across different areas, once it has been found that SRFs are highly dependent on the relative magnitude of earthquake and wind forces. This measure could be more effective than modifying load combination factors for wind resisting design when seismic load counts as additional variable load.The proposed method was verified with the conventional and ty- pical low-rise and medium-rise buildings by using the same foundation type, hence addressing SSI effects across different case studies. We re- cognise the fact that high-rise buildings take higher risks under wind actions due their aero elasticity, thus a future prospect would in- vestigate the effect of multi-hazard scenarios on foundation types that are proper of high-rise buildings

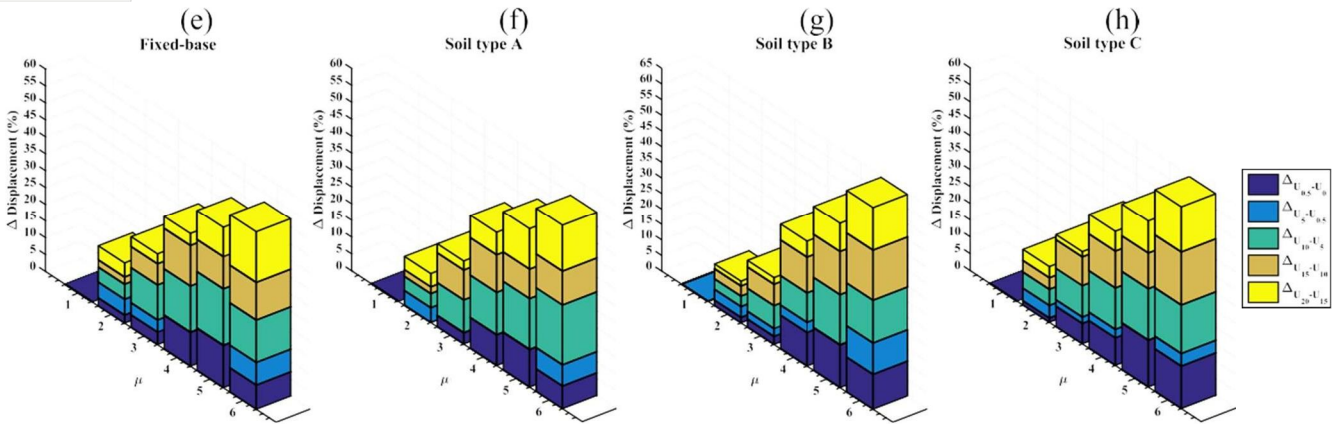

Fig. 11. Rate of change (%) in displacement related to different wind velocity intervals. (a)-(d) results of the 5-storey results of the 8-storey building with fixed-base and soil types A to C.

REFERENCES

[1] Ashiru Muhammad, Chhavi Gupta, Ibrahim B. Mahmoud "Comparative analysis of Seismic Behaviour of Multi-storey Composite Steel and Conventional Reinforced Concrete Framed Structures". (2015)
[2] S.A. Raji, A.A. Bello, O.I. Adeyanju, O.L. Tazou "Analysis of a Six Storey Steel Frame Structure using AutodeskRevit, Staadpro and SAP2000". (2017)
[3] Mahesh Suresh Kumawat and L.G. Kalurkar "Analysis and Design of multistory building using composite structure". (2014)
[4] Aman, Manjunath Nalwadgi, Vishal T, Gajendra "Analysis and design of multistorey building by using STAAD Pro". (2016)
[5] V Ratna Priya and N jitendra Babu "Seismic reaction of building frame under various zones considering flexible and rigid supports". (2017)
[6] Girum Mindaye and Shaik Yajdani "Seismic Analysis of a Multi- storey RC Frame Building in Different Seismic Zones". (2001)
[7] Ashis Debashis Behera, K.C. Biswal "3DAnalysis Of Building Frame Using Staad Pro." (2001)
[8] Sudhir K. Jain and R.K. Ingle "Explanatory Examples for Ductile Detailing Of RC Building".
[9] Sudhir K Jain, H.J.Shah "Design Example of a Six Storey Building".
[10] P. Jayachandran and S. Rajasekaran "Structural Design of Multi- story Residential Building for in Salem, India". (2006)
[11] V.Varalakshmi, G. Shiva Kumar and R. Sunil Sarma "Analysis and Design of G+5 residential building". (2006)

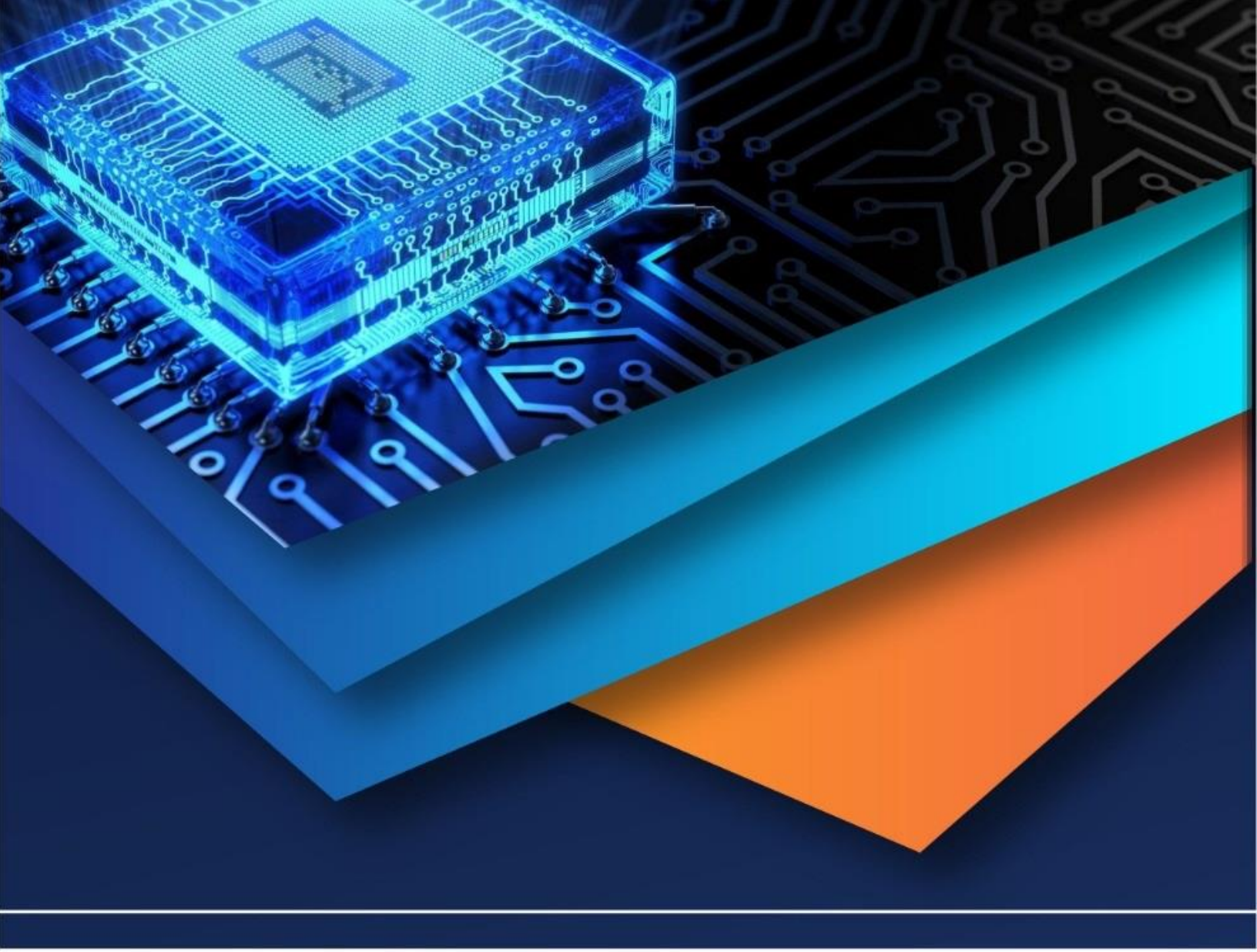

10.22214/IJRASET

45.98

IMPACT FACTOR: 7.129

IMPACT FACTOR: 7.429

INTERNATIONAL JOURNAL FOR RESEARCH

IN APPLIED SCIENCE & ENGINEERING TECHNOLOGY